

# Modeling and Technical Analysis of Solar Tracking System to Find Optimal Angle for Maximum Power Generation using MOPSO Algorithm

H. Pourderogar<sup>1</sup>, H. Harasii<sup>2</sup>, R. Alayi<sup>3</sup>, S. H. Delbari<sup>4</sup>, M. Sadeghzadeh<sup>4\*</sup>, and A. Javaherbakhsh<sup>5</sup>

1. Energy Higher Education Institute of Saveh, Saveh, Iran

2. Islamic Azad University, Ardabil, Iran

3. Department of Mechanical Engineering, Germi Branch, Islamic Azad University, Germi, Iran

4. Faculty of New Sciences and Technologies, University of Tehran, Tehran, Iran

5. School of Electrical Engineering, Iran University of Science and Technology, Tehran, Iran

Receive Date 24 March 2020; Revised 12 May 2020; Accepted Date 19 May 2020

\*Corresponding authors: milad.sadeghzadeh@gmail.com (M. Sadeghzadeh)

## Abstract

In this work, we aim to determine the optimal performance characteristics of a solar tracking system in order to maximize the power generation through using the MOPSO algorithm. Considering the sun path during a day, the necessity of using solar tracking systems to achieve the maximum power output from photovoltaic (PV) panels is investigated. The solar tracking system allows the PV arrays to follow sunlight all day long. The unidirectional tracking system follows the sun path, thereby, optimizing the angular motion of the PV arrays relative to the sun resulting in a higher power generation. In order to evaluate the performance of a PV system, the total solar radiation is calculated first for both the fixed and unidirectional tracking systems. Analyzing the results indicates that for June 20<sup>th</sup>, the power generation of the PV module equipped with a unidirectional tracker is 35% higher than the fixed PV module. The optimal value of the declination angle, Azimuth, and arrays' tilting angles in a unidirectional tracking system calculated using the MOPSO algorithm are 31.8°, 178.2° and 85.1°, respectively.

**Keywords:** Solar tracker, MOPSO algorithm, Photovoltaic systems, Energy analysis.

## 1. Introduction

In today's world, energy is a primary requirement for the human activities, and dependence on the fossil fuels has been increased more than ever, up to 90% of the global energy consumption supplied from these conventional resources [1]. The limited resources of fossil fuels and the problems associated with greenhouse gas emissions urge attention to employ clean and renewable energy sources [2, 3]. Therefore, the decline in fossil resources has globally propelled the utilization of environmentally friendly renewable energies. Among the renewable resources, solar energy has significantly progressed in the recent years [4, 5]. Distributed Generation (DG) and connecting the produced power to the regional network has been introduced as a practical way for environment protection. This application of power production can be used at the end point of consumption or by proposing a distribution grid through establishment of smart grids and micro-grids to achieve socio-economic benefits for the end-users. In terms of introducing the renewable energy sources for being utilized in smart grid networks, the area of focus is on the photovoltaic (PV) systems [6–9]. The PV

module produces zero emission electricity by converting solar power into electricity. The PV systems are becoming more and more attractive between the people and industries. For example, 550,000 new PV farms were constructed in Italy from 2005 to 2013. However, the PV cost is not still competitive with other conventional electricity production technologies. The PV efficiency is defined as a function of output electricity and receiving solar irradiation on panels [10, 11]. Many researchers throughout the world have placed a premium on improving the efficiency of PV modules to benefit the most out of the solar energy. For this aim, the PV technology in parallel to the control systems are investigated to maximize the output efficiency and the output power in every environmental condition. Currently, commercially Si-panels including mono-crystalline-Si and twin-Si are the most utilized panels with a highest efficiency of 17-18%. All the PV systems are armed with a Maximum Power Point Tracker (MPPT). This feature helps PV to work at its maximum power all the time through applying various MPPT plans. In addition, installing a sun-

tracking system in a solar system could ameliorate the overall efficiency [12]. Besides, aligning the PV panel with the direction of solar irradiance has optimized the PV efficiency since the amount of receiving irradiance where “direct” to the panel has been reached to its maximum. Hence, the output efficiency of the PV panel can be increased by tuning its direction to be always perpendicular in relation to the sun by adding a solar tracker. Thus an efficient solar energy collector can be yielded by setting a suitable tracking control system [13]. On the other hand, it is true that installing a tracker increases the daily and, in similar, the yearly output but this equipment is expensive and also makes the overall system more and more complicated [9]. The final utilization target and the latitude of the site are the two factors that affect the optimal angle [14, 15]. Up to date, two conventional tracking systems are commercially available worldwide, namely single-axis tracker (east to west) and dual-axis tracker (east to west + tilt angle) [9]. Recently, several design approaches have been introduced for the solar tracking systems [16–22]. It can be concluded that the major limitations toward the solar tracking models are the sunlight sensing, initial mode of the solar PV panel, control unit design, evaluating the efficiency, and motorizing the tracker. Therefore, the performance of fixed PV arrays employing the unidirectional tracking system is evaluated and optimized using the MOPSO algorithm due its fast convergence and also less required computation.

**2. Materials and Methods**

The amount of solar energy received at the Earth varies depending on the latitude, altitude, atmospheric phenomenon, etc. Therefore, it is required to determine the geographical coordinate of a given area to calculate the solar irradiance data on a horizontal or any arbitrary surface with varying slope and direction, located in that area, on a monthly and annual basis.

Knowing the sun’s trajectory is beneficial to determine the optimal tracking angle of PV modules in which power generation is maximum. The angle of solar radiation varies constantly during the day and changes the irradiance reaching the surface of a given area. Thus to ensure the maximum solar radiation flux absorbed by PV modules, the instantaneous position of the sun in the sky is required.

Reducing COE and improving the efficiency of solar PV panels are of the researchers' interests. These are achieved through optimal utilization of solar irradiance by implementing solar tracking systems for PV arrays.

The direct (beam) portion of the solar irradiance reaching the earth’s surface is calculated using the following equation:

$$I_B = A e^{-km} \tag{1}$$

Where A is an apparent extra-terrestrial solar insolation, and is determined by equation (2), in which n is the day number.

$$A = 1160 + 75 \sin\left[\frac{360}{365}(n - 275)\right] \text{ (W / m}^2\text{)} \tag{2}$$

In equation (1) , K and M are the atmospheric optical depth and the air mass ratio, respectively, which are given as follow [23, 24]:

$$k = 0.174 + 0.035 \sin\left[\frac{360}{365}(n - 100)\right] \tag{3}$$

$$m = \frac{1}{\sin \beta} \tag{4}$$

Where b is the altitude angle of the sun, and is calculated using equation (5); L, H, and d are latitude, hour, and solar declination angles, respectively.

$$\sin \beta = (\cos L \times \cos \delta \times \cos H) + (\sin L \times \sin \delta) \tag{5}$$

The direct beam insolation absorbed by the collector is given by:

$$I_{BC} = I_B \cos \theta \tag{6}$$

in which q is the incidence angle between the normal to the panel’s face and the incoming solar beam radiation, and is given as follows [25]:

$$\cos q = \cos b \times \cos(f_s - f_c) \cdot \sin g + \sin b \times \cos d \tag{7}$$

$f_s$  ,  $f_c$ , and g are solar azimuth angle, collector azimuth angle and collector tilt angle, respectively. The solar azimuth and declination angles are represented in equations (8) and (9) [6] .

$$\sin \phi_s = \frac{\cos \delta \times \sin H}{\cos \beta} \tag{8}$$

$$\delta = 23.45 \times \sin\left[\frac{360}{35}(n - 81)\right] \tag{9}$$

In equation (9), the hour angle is given as follows:

$$H = 15(ST - 12) \tag{10}$$

where ST is the solar time.

The solar time differs from the clock time (CT), and it depends on the local longitude, local time meridian, clock time, and equation of time (E), as represented in equation (11) .

$$\begin{aligned} \text{Solar Time (ST)} = \\ \text{Clock Time (CT)} \\ + \frac{4\text{min}}{\text{degree}} (\text{Local Time Meridian} - \\ \text{Local Longitude})^\circ \\ + E(\text{min}) \end{aligned} \tag{11}$$

$$\begin{aligned} E = 229.2(0.000075 + 0.001868\cos B \\ - 0.032077 \sin B - 0.14615\cos 2B \\ - 0.04089\sin 2B) \end{aligned} \tag{12}$$

where B is equal to:

$$B = (n - 1) * \frac{360}{365} \tag{13}$$

Similarly, the diffuse insolation on a horizontal surface is calculated using the following equation:

$$I_{DH} = C.I_B \tag{14}$$

where C is the sky diffuse factor, and is estimated as follows:

$$C = 0.095 + 0.04 \sin \left[ \frac{360}{365} (n - 100) \right] \tag{15}$$

According to equation (14), the solar irradiance absorbed by the collector is calculated using equation (16) .

$$I_{DC} = I_{DH} \left( \frac{1 + \cos \delta}{2} \right) = I_B C \left( \frac{1 + \cos \delta}{2} \right) \tag{16}$$

Additionally, the reflected portion of the solar insolation reaching the collector surface is obtained by equation (17).

$$I_{RC} = \rho I_B (\sin \beta + C) \left( \frac{1 - \cos \delta}{2} \right) \tag{17}$$

where r is the ground reflectance.

Consequently, the total rate at which radiation is absorbed at a collector’s surface is the sum of its

direct beam, diffuse, and reflected components given in equations (6), (16), and (17), respectively.

$$G = I_{BC} + I_{DC} + I_{RC} \tag{18}$$

In a single axis PV array, the panel’s tilt angle follows the sun from east in the morning to the west in the evening, and  $f_C$  is assumed to be constant. The direct, diffuse, and radiated portions of radiation on a PV array equipped with a unidirectional tracking system are given as follow:

$$I_{BC} = I_B \cos \delta \tag{19}$$

$$I_{DC} = C I_B \left[ \frac{1 + \cos(90^\circ - \beta + \delta)}{2} \right] \tag{20}$$

$$I_{RC} = \rho (I_{BH} + I_{DH}) \left[ \frac{1 - \cos(90^\circ - \beta + \delta)}{2} \right] \tag{21}$$

**2.1. Modeling a photovoltaic cell**

The PV module used in this work is SUNPOWER X21-345, whose I-V curve is shown in figure 1. Also the module’s characteristics including efficiency, maximum values of power, voltage and current, open-circuit voltage, short-circuit current, number of cells per module, and area of the module are presented in table 1.

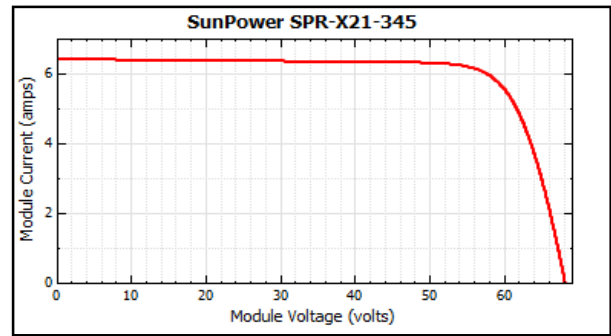


Figure 1. I-V curve of the SUNPOWER X21-345 module.

Figure 2 shows the efficiency curve of the SMA America ST36-240 (240V) converter used in the model. The technical data of the converter such as maximum AC output at reference condition, maximum DC input to the converter, DC power required for operation, etc. is provided in table 2. After specifying the module type and the converter, the proposed PV system is modeled to compare the power produced at a fixed-tilt and a unidirectional tracker module. A single diode PV module (shown in figure 3) is used for this purpose. According to this figure, the output current is obtained by using equation (22).

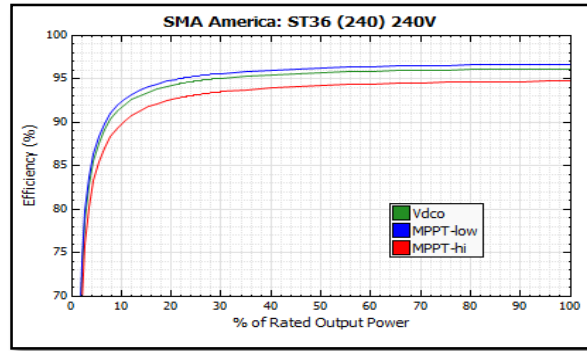


Figure 2. Efficiency curve of the SMA America: ST36-240 (240 V).

Table 1. Characteristics of the PV module.

| Parameter             | Unit | Value  | Parameter       | Unit           | Value |
|-----------------------|------|--------|-----------------|----------------|-------|
| Efficiency ( $\eta$ ) | %    | 21.15  | $V_{ac}^{DC}$   | V              | 68.2  |
| $P_{max}^{DC}$        | W    | 344.94 | $I_{SC}$        | A              | 6.39  |
| $V_{max}^{DC}$        | V    | 57.3   | Number of cells | -              | 96    |
| $I_{max}^{DC}$        | A    | 6.02   | Area            | m <sup>2</sup> | 1.631 |

Table 2. Technical data of the ST36-240 (240 V) converter.

| Parameter                     | Unit     | Value   |
|-------------------------------|----------|---------|
| Max. apparent AC power        | $W_{ac}$ | 36000   |
| Max. PV array power           | $W_{dc}$ | 37453.9 |
| Initial input power           | $W_{dc}$ | 194.96  |
| AC power consumption at night | $W_{dc}$ | 0.6     |
| Output voltage                | $V_{ac}$ | 240     |
| Max. input voltage            | $V_{dc}$ | 600     |
| Max. input current            | $A_{dc}$ | 150     |
| Min. operating voltage        | $V_{dc}$ | 250     |
| Avg. operating voltage        | $V_{dc}$ | 309.917 |
| Max. operating voltage        | $V_{dc}$ | 480     |

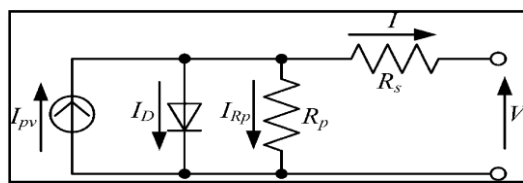


Figure 3. Electric circuit of the PV module.

$$I = I_{pv} - I_o \times \left[ \exp\left(\frac{V + IR_s}{\alpha \times N_s \times V_t}\right) - 1 \right] - \frac{V + IR_s}{R_p} \quad (22)$$

where  $I_o$  is the reverse saturation current of diode,  $a$  is the ideal coefficient, and  $N_s$  is the number of cells in series. Additionally,  $V_t$  is the thermal voltage, and is obtained by equation (23).

$$V_t = \frac{K \times T}{q} \quad (23)$$

in which  $T$  is the junction temperature (K),  $q = 1.60217646 \times 10^{-19} C$  is the electric charge, and  $K = 1.3806503 \times 10^{-23} J/K$  is the Boltzmann constant. In order to investigate the single diode PV module model, the following cases can be considered:

1. For the short-circuit (SC) condition at temperature  $T$  ( $V = 0, I = I_{SC}(T)$ ):

$$I_{sc}(T) = \frac{R_p}{R_s + R_p} \times \left[ I_{pv} - I_o \left( \exp\left(\frac{I_{sc}(T) \times R_s}{\alpha \times N_s \times V_t(T)}\right) - 1 \right) \right] \quad (24)$$

2. For the open-circuit condition ( $I = 0, V = V_{OC}(T)$ ):

$$V_{oc}(T) = R_p \times \left[ I_{pv} - I_o \left( \exp\left(\frac{V_{oc}(T)}{\alpha \times N_s \times V_t(T)}\right) - 1 \right) \right] \quad (25)$$

Substituting  $I = I_{mp}(T)$  and  $V = V_{mp}(T)$  into the corresponding equations, the maximum power equation is written as follows:

$$P_{mp}(T) = \frac{R_p \times V_{mp}(T)}{R_s + R_p} \times \left[ I_{PV} - I_0 \left( \exp \left( \frac{V_{mp}(T) + I_{mp}(T)R_s}{\alpha \times N_s \times V_t(T)} \right) - 1 \right) - \frac{V_{mp}(T)}{R_p} \right] \quad (26)$$

where  $G_n$  and  $I_{PV,n}$  are the solar insolation intensity and the current under the standard test condition (STC).  $K_{I_{SC}}$  (mA/°C) is the short-circuit thermal coefficient and  $DT = T - T_n$  is the temperature difference between STC and the real condition.

**2.2. Optimization method**

The multi-objective particle swarm optimization (MOPSO) is similar to the PSO algorithm, except that it has two or more objective functions. Figure 4. shows the MOPSO algorithm flowchart. Table 3 shows the parameters and the values used in the optimization process.

**Table 3. Optimization parameters and their values for the model.**

| Parameter      | Value |
|----------------|-------|
| No. population | 100   |
| Max. iteration | 160   |
| C <sub>1</sub> | 2     |
| C <sub>2</sub> | 2     |

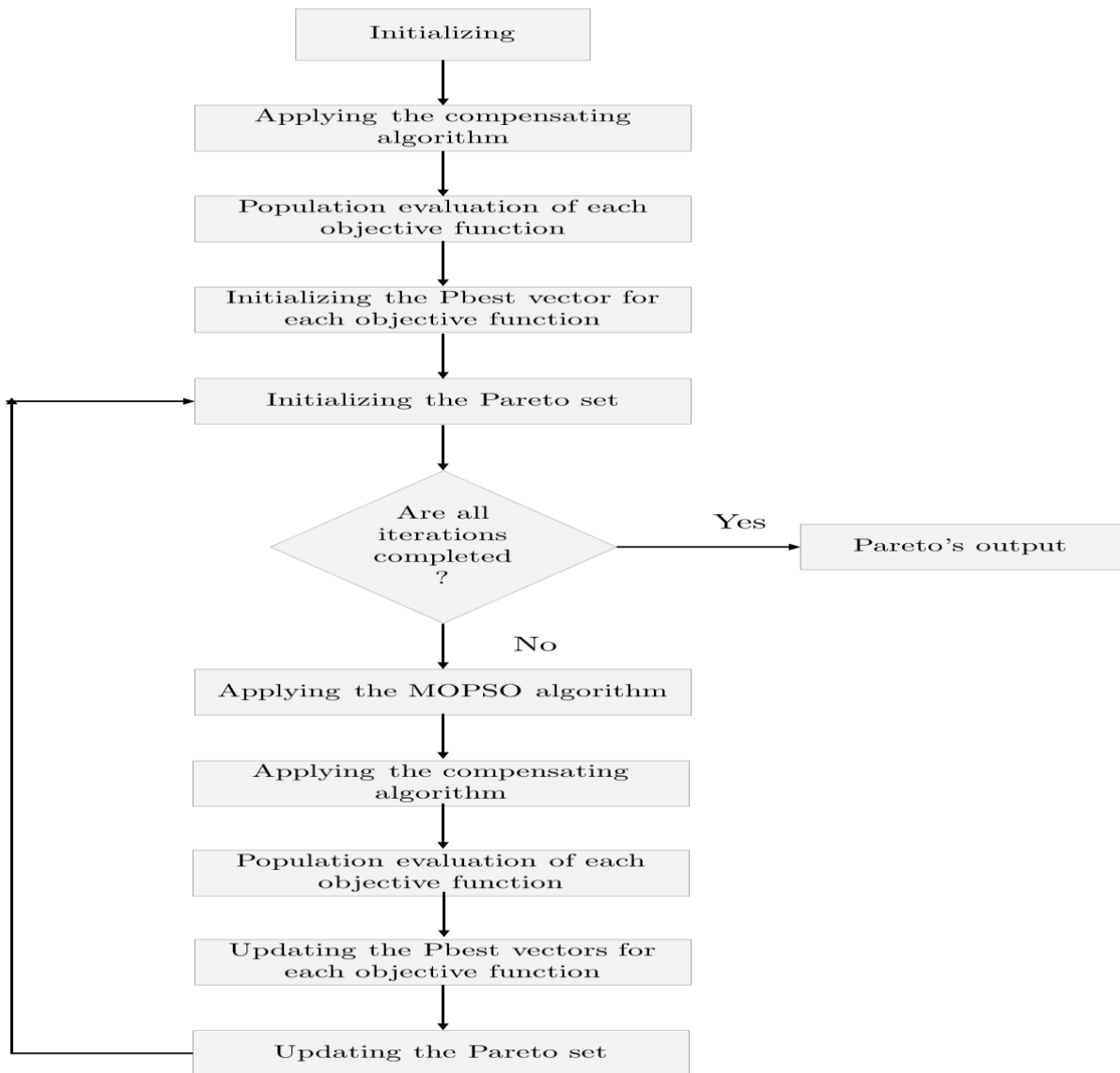


**Figure 4. The MOPSO algorithm flowchart.**

**2.3. Objective functions**

In this work, two objective functions were used to optimize the performance of the PV system. The

equations along with their constraints are represented as follow:

Obj. Function 1

Object Function 1:  $Max (G_1(\delta, \varphi_c))$

$$\text{Subject to: } \begin{cases} \delta_{min} < \delta < \delta_{max} \\ \varphi_{c,min} < \varphi_c < \varphi_{c,max} \end{cases}$$

where  $d_{min}$  and  $d_{max}$  are the lower and upper bounds of  $Z$ , which are equal to  $0^\circ$  and  $90^\circ$ , respectively. Similarly,  $f_{c,min}$  and  $f_{c,max}$  are the upper and lower bounds of  $f_c$ , which are equal to  $0^\circ$  and  $360^\circ$ , respectively.

Obj. Function 2

Object Function 2:  $Max (G_2(\gamma))$

$$\text{Subject to: } \gamma_{min} < \gamma < \gamma_{max}$$

$\gamma$  is the collector's tilting angle of the unidirectional tracking system varying from  $0^\circ$  to  $90^\circ$ ;  $0^\circ$  and  $90^\circ$  represent  $\gamma_{min}$  and  $\gamma_{max}$ , respectively.

### 3. Results

#### 3.1. Technical analysis of solar tracking system

In order to assess the performance of the PV module, first, the total solar irradiance on the collector for both the fixed and moving modules is to be determined using the equations provided in the previous section. The key parameters affecting the absorption of solar insolation are the collector azimuth angle  $f_c$  and the solar declination angle  $d$ . Maintaining these angles near their optimal values guarantee the highest level of annual electricity production. Generally,  $d$  is equal to the latitude of an area wherein the PV system is installed. Additionally,  $f_c$  is set to be  $180^\circ$  or adjusted facing the equator. The total solar insolation ( $G$ ) was calculated for two particular days of the year, February 19<sup>th</sup> ( $n=50$ ) and June 20<sup>th</sup> ( $n=171$ ). Figures 5 and 6 demonstrate the  $G$  values with  $G_1$  and  $G_2$  representing the fixed and the solar tracking PV systems, respectively.

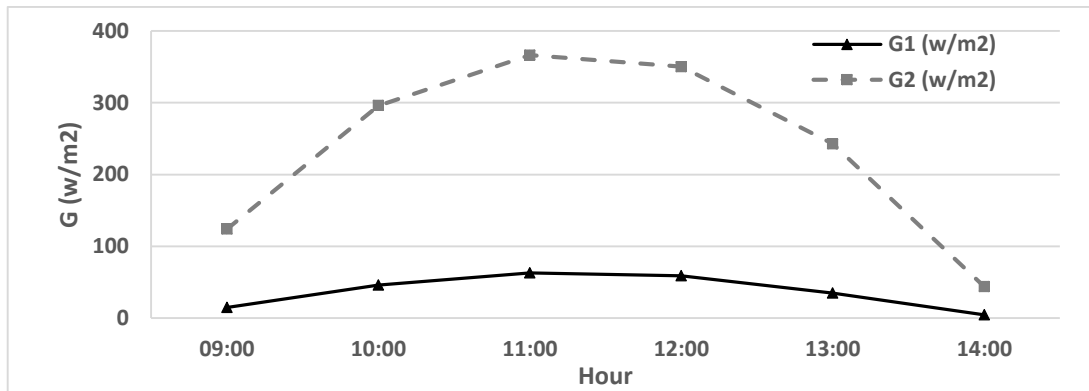


Figure 5. Total solar insolation reaching the fixed PV module ( $G_1$ ) and the PV module with solar tracking system ( $G_2$ ) on Feb 19th in Tehran.

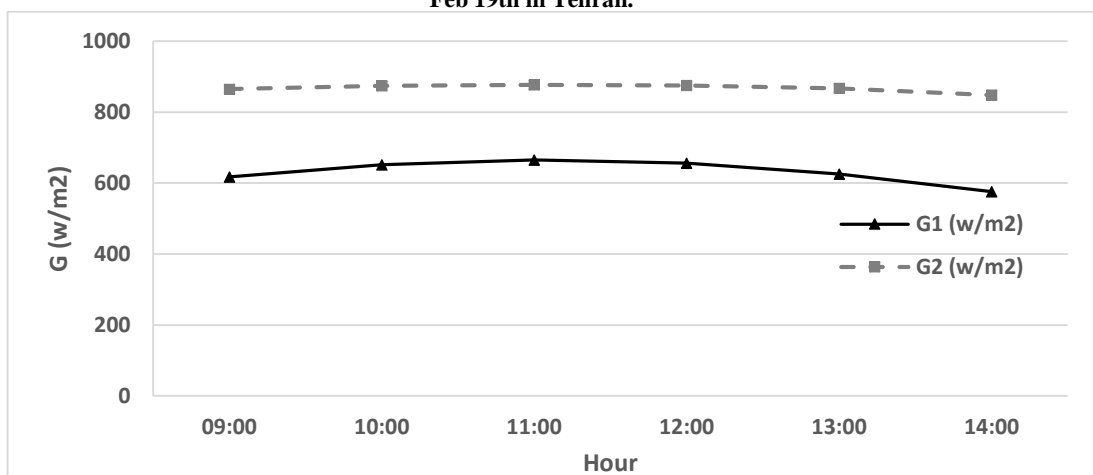


Figure 6. Total solar insolation reaching the fixed PV module ( $G_1$ ) and the PV module with solar tracking system ( $G_2$ ) on Jun 20th in Tehran

The I-V and P-V curves of the two proposed systems were also investigated using the sensitivity analysis. Figures 7 and 8 show the I-V and P-V

characteristic curves of the fixed-tilt and the uniaxial tracker PV module at noon on Feb 19<sup>th</sup> mounted in Tehran. Similarly, the characteristic

curves of the two PV systems on Jun 20<sup>th</sup> at noon are shown in Figures 9 and 10. The PV module equipped with a unidirectional tracking system has a higher output current, thus producing a higher level of power than the fixed PV module. The maximum electricity produced by the fixed-tilt and the unidirectional tracker PV module on Jun 20<sup>th</sup> at noon were 211.41 W and 285.36 W, respectively. The PV module with the tracker generates 35% more electricity than the fixed module. On Feb 19<sup>th</sup>, the difference is even more pronounced as the former produces 8 times higher electricity than the latter. The output of the fixed and the tracker-mounted PV modules on Feb 19th are 12.96 W and 108.03 W, respectively.

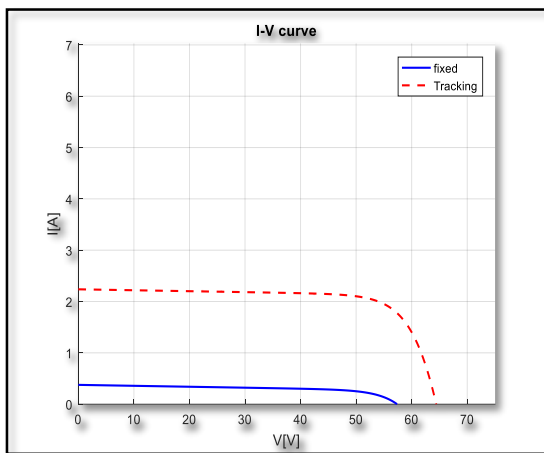


Figure 7. I-V curve of the fixed module (solid line) and the module with unidirectional solar tracker (dotted line) mounted in Tehran on Feb 19th at noon.

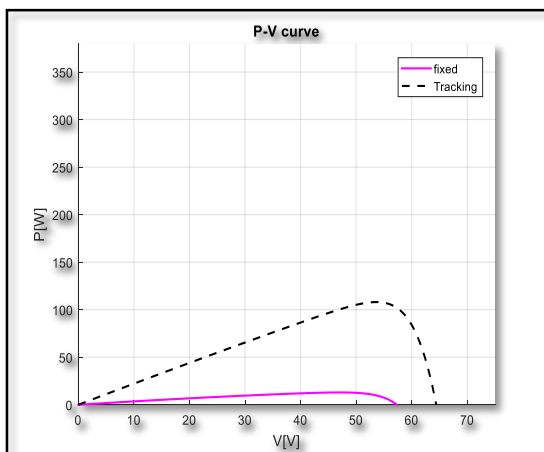


Figure 8. P-V curve of the fixed module (solid line) and the module with unidirectional solar tracker (dotted line) mounted in Tehran on Feb 19th at noon.

In a larger scale, a PV farm constitutes 20 modules in 10 rows and 2 columns with a total surface area of 32.962 m<sup>2</sup> modeled in a whole year to compare the system performance in the fixed and solar

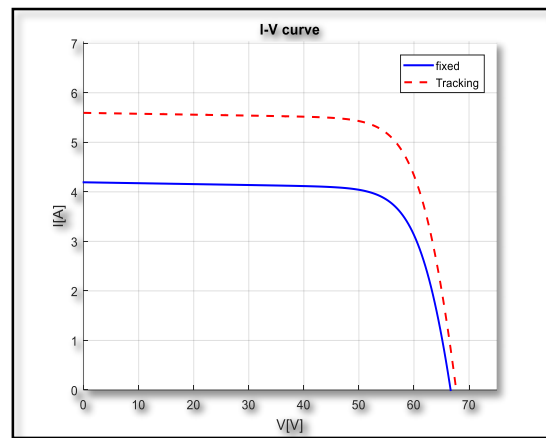


Figure 9. I-V curve of the fixed module (solid line) and the module with unidirectional solar tracker (dotted line) mounted in Tehran on Jun 20th at noon.

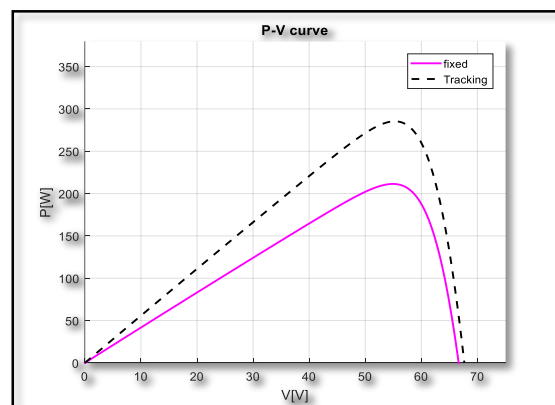


Figure 10. P-V curve of the fixed module (solid line) and the module with unidirectional solar tracker (dotted line) mounted in Tehran on Jun 20th at noon.

tracking modes ( $d=45^\circ$ ). Figure 11 shows the annual electricity generated in the fixed and tracking modes, which are 12161 kWh and 15090 kWh, respectively. A 24 % increase in the total electricity generation is achieved through using the tracking system.

### 3.2. Optimization of solar PV system

The objective functions and constraints defined in Section 2.2 were optimized using the MOPSO algorithm in MATLAB to find the optimal values for  $d$ ,  $f_c$ , and  $g$  for the proposed PV system, respectively. By substituting the optimal values for the mentioned variables into the characteristic equations of the PV system, the total solar insolation and the annual electricity produced were calculated again. The results obtained indicate that for the maximum power output,  $d$ ,  $f_c$ , and  $g$  should be  $31.8^\circ$ ,  $178.2^\circ$  and  $85.1^\circ$ , respectively. The annual electricity generated by the fixed-tilt PV system configured with the default and optimal angles is shown in figure 12. Similarly, the corresponding values for the typical and optimized uniaxial solar tracker is depicted in figure 13.

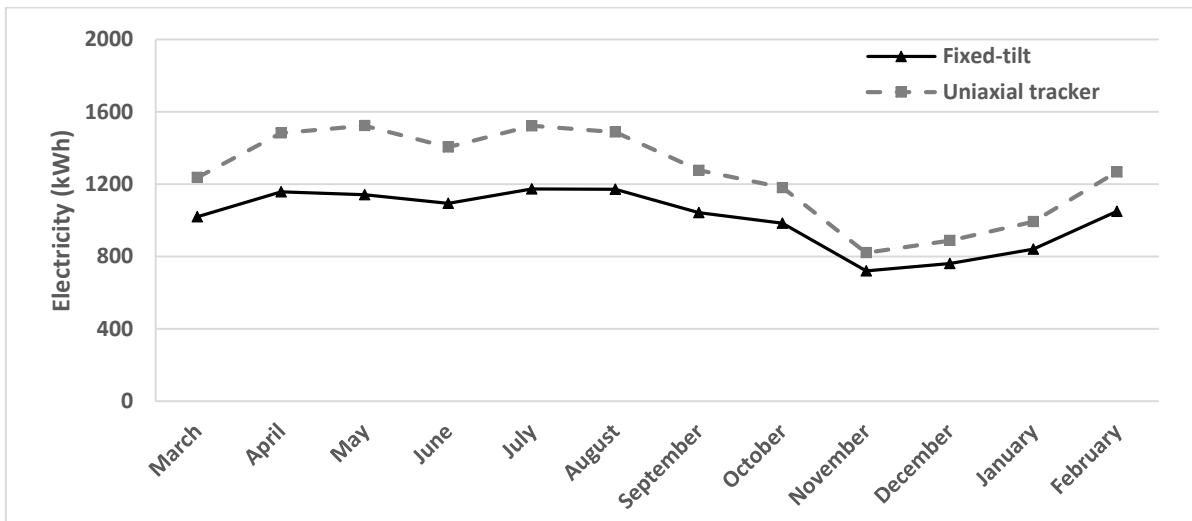


Figure 11. Annual electricity generated by the fixed and the unidirectional solar tracking PV arrays mounted in Tehran.

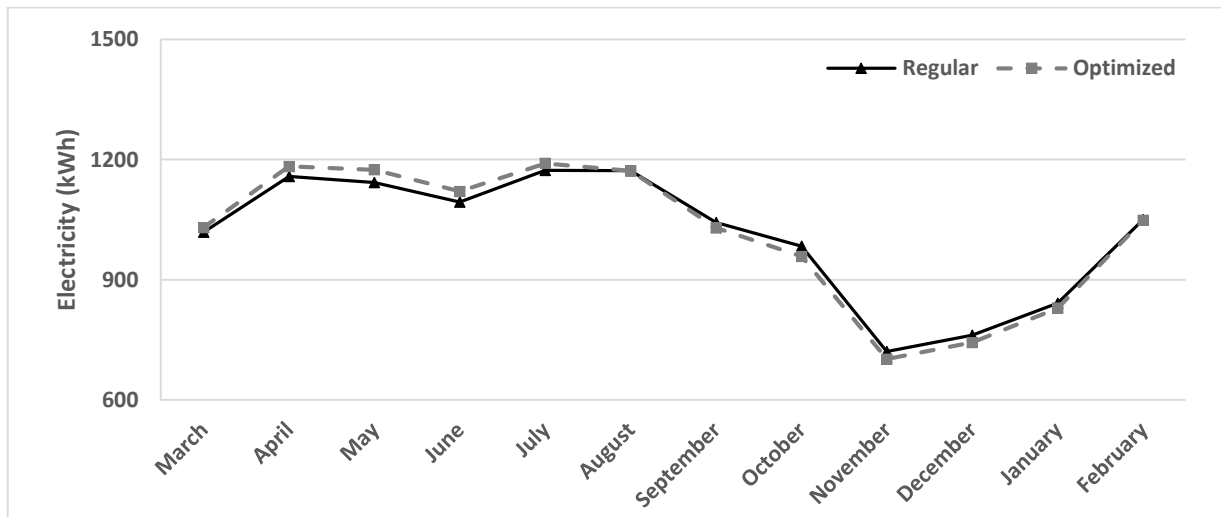


Figure 12. Comparison between the annual generated electricity for the typical and the optimized fixed-tilt PV system.

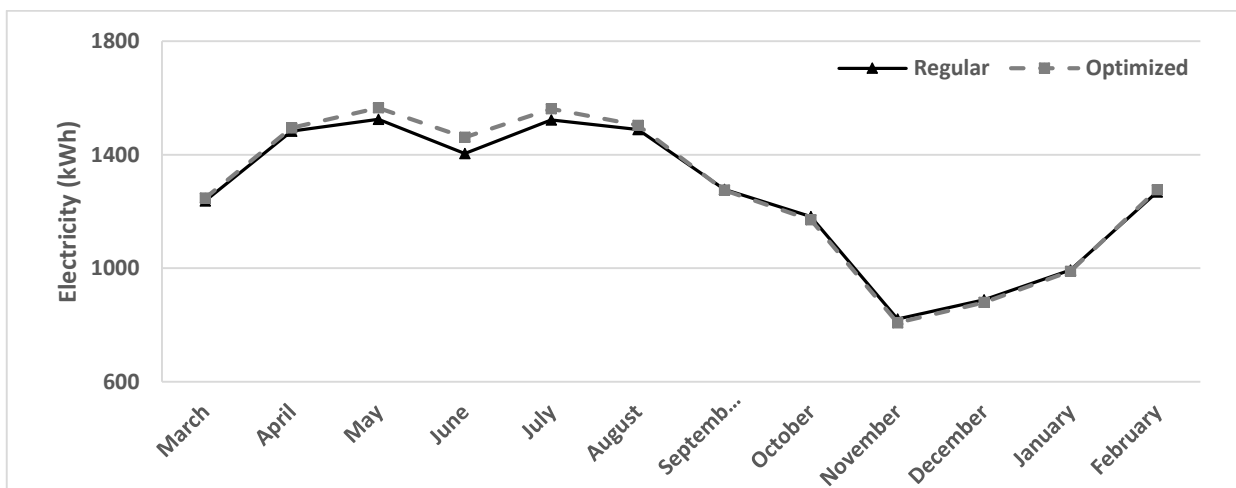


Figure 13. Comparison between the annual generated electricity for the typical and the optimized uniaxial tracker PV system.

Based on figure 12, the optimized fixed-tilt PV system produces 0.17% higher electricity than the regular one. Moreover, the increased energy output of the uniaxial tracker PV system after optimization is around 0.94%.

According to figure 14, the MOPSO algorithm converges roughly at the 60<sup>th</sup> iteration. Additionally, figures 15 to 22 illustrate the I-V and P-V characteristic curves of both the fixed-tilt and the unidirectional tracker PV systems before and after optimization on Feb 19<sup>th</sup> and Jun 20<sup>th</sup> at noon. It can be stated that the optimized PV systems have a higher output power than the regular systems.

The results of sensitivity analysis determine that the maximum output power of the optimized and regular fixed PV system on Jun 20<sup>th</sup> are 221.01 W and 211.41 W, respectively, which demonstrate a 4.5% increase (figures 16 and 18). For the uniaxial tracker PV system, the maximum output power is 296.07 W and 285.36 W, respectively, before and after the optimization rendering 3.7% improvement in performance (figures 20 and 22). On Feb 19<sup>th</sup>, the fixed PV system produces 12.96 W and 15.54 W before and after the optimization. Similarly, the optimized and regular uniaxial tracker PV system outputs are 108.037 W and 128.17 W, respectively. Consequently, the optimization process results in 19.91% and 15.85% increases, respectively, in the maximum power output compared to the corresponding values of the regular fixed-tilt and the regular uniaxial tracker PV systems.

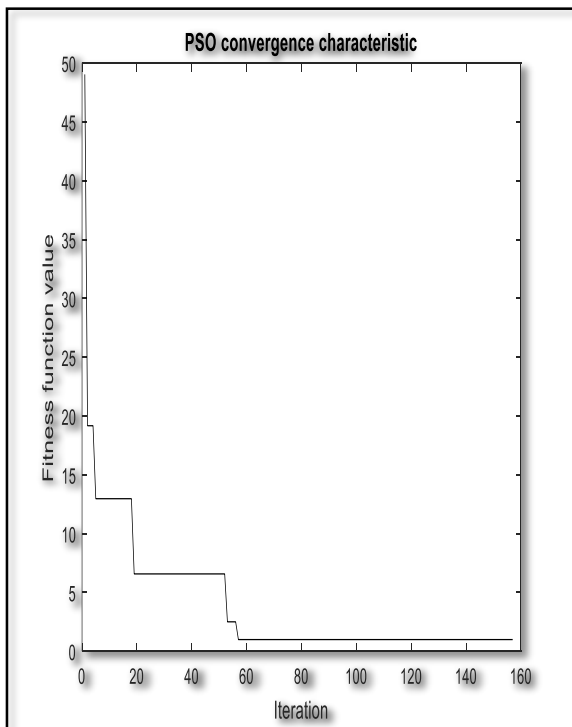


Figure 14. Convergence trend of the MOPSO algorithm.

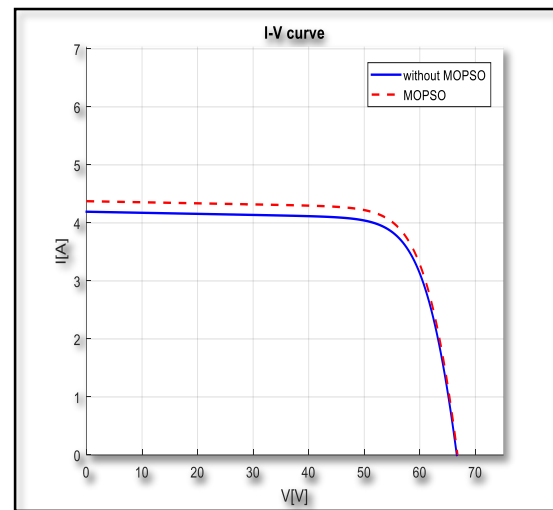


Figure 15. I-V curve of the fixed-tilt PV system before and after optimization on June 20th at 12:00 PM mounted in Tehran.

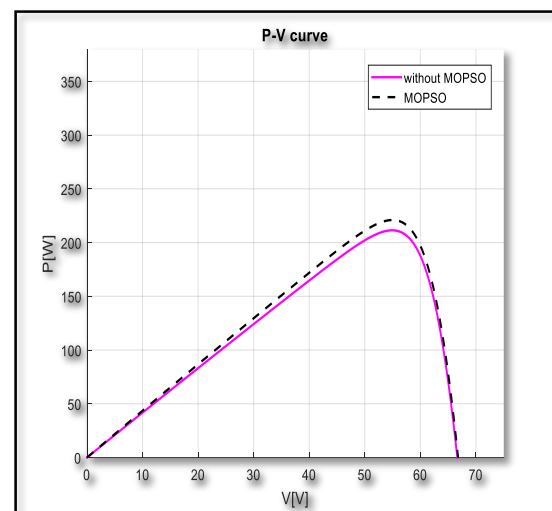


Figure 16. P-V curve of the fixed-tilt PV system before and after optimization on June 20th at 12:00 PM mounted in Tehran.

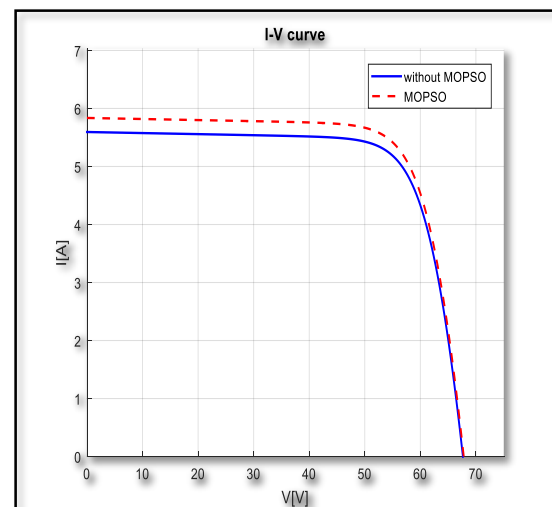


Figure 17. I-V curve of the uniaxial tracker PV system before and after optimization on June 20th at 12:00 PM mounted in Tehran.

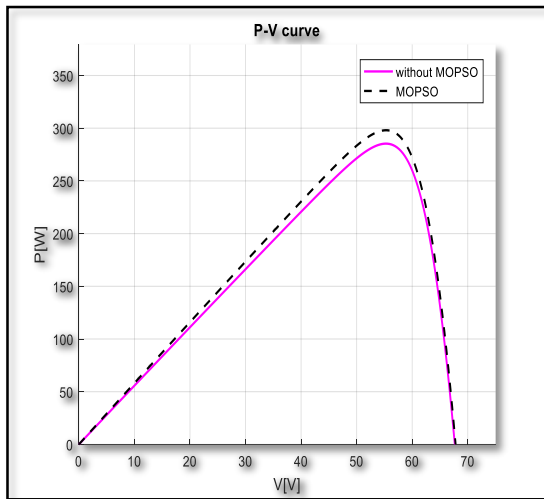


Figure 18. P-V curve of the uniaxial tracker PV system before and after optimization on June 20th at 12:00 PM mounted in Tehran.

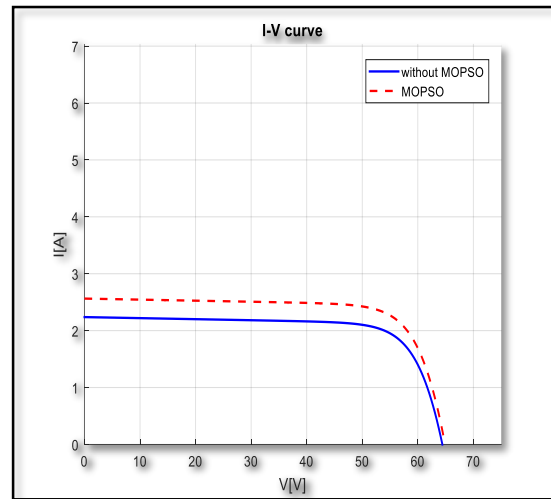


Figure 21. I-V curve of the uniaxial tracker PV system before and after optimization on Feb 19th at 12:00 PM mounted in Tehran.

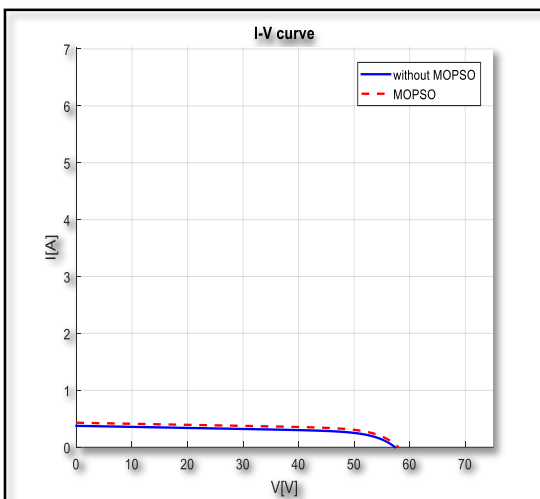


Figure 19. I-V curve of the fixed-tilt PV system before and after optimization on Feb 19th at 12:00 PM mounted in Tehran.

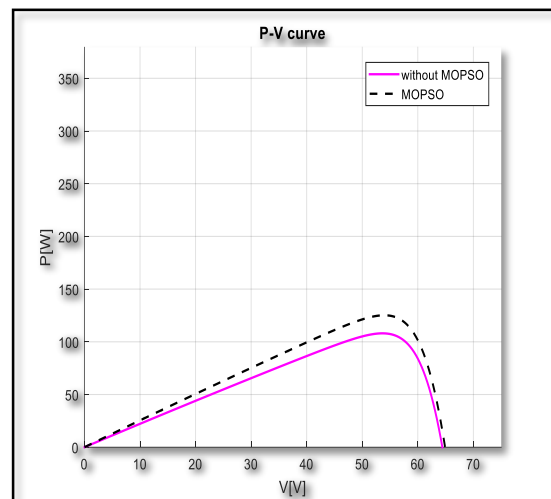


Figure 22. P-V curve of the uniaxial tracker PV system before and after optimization on Feb 19th at 12:00 PM mounted in Tehran.

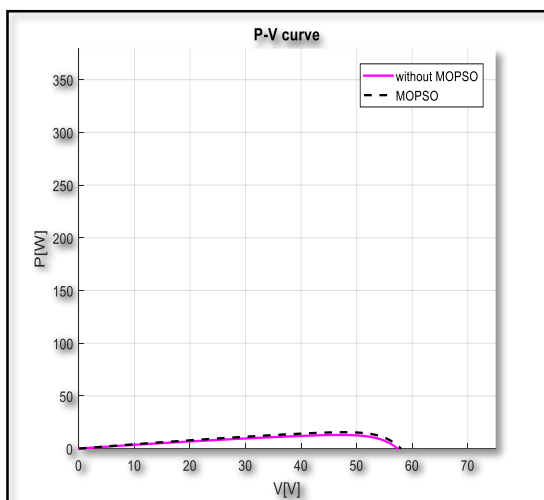


Figure 20. P-V curve of the fixed-tilt PV system before and after optimization on Feb 19th at 12:00 PM mounted in Tehran.

#### 4. Conclusion

In this work, a technical analysis was conducted to evaluate the performance improvement of fixed PV arrays using unidirectional solar tracking systems. The MOPSO algorithm was chosen to optimize the system's performance characteristics using the climatic data of Tehran as a case study. The total solar irradiance was calculated for both the fixed-tilt and the unidirectional tracker PV module to compare their performance. The calculation was performed for two distinctive dates, namely Feb 19<sup>th</sup> and Jun 20<sup>th</sup>, using the regional latitude and 180° southward as the default values for the declination and the solar collector azimuth angles, respectively.

- The results obtained show an increase in the power output of the uniaxial tracker PV

module with respect to the fixed-tilt configuration.

- On Jun 20<sup>th</sup>, the PV module mounted on a tracker generates 35% higher electricity compared to the fixed PV module. The former produces 8 times higher electricity on Feb 19<sup>th</sup>.
- The arrangement of 20 PV modules with the total surface area of 32.62 m<sup>2</sup> equipped with a tracking system results in a 24% increase in the annual electricity generation. In this step, the total solar irradiance reaching the surface of the PV panel is considered as a function of the declination, collector azimuth, and collector tilting angles optimized under the pre-defined constraints using MATLAB. Consequently, the optimal angles are 31.8°, 178.2°, and 85.1°, respectively.
- After optimization, the annual rate of electricity production improves by 0.17% and 0.94% for the fixed-tilt and the uniaxial tracker PV systems, respectively.

## References

- [1] Ahmadi MH, Alhuyi Nazari M, Sadeghzadeh M, Pourfayaz F, Ghazvini M, Ming T, et al. Thermodynamic and economic analysis of performance evaluation of all the thermal power plants: A review. *Energy Sci Eng* 2019; 7:30–65.
- [2] Rezaei MH, Sadeghzadeh M, Alhuyi Nazari M, Ahmadi MH, Astarai FR. Applying GMDH artificial neural network in modeling CO<sub>2</sub> emissions in four nordic countries. *Int J Low-Carbon Technol* 2018:1–6.
- [3] Ahmadi MH, Ghazvini M, Sadeghzadeh M, Alhuyi Nazari M, Kumar R, Naeimi A, et al. Solar power technology for electricity generation: A critical review. *Energy Sci Eng* 2018:1–22.
- [4] Ghorbani B, Mehrpooya M, Sadeghzadeh M. Developing a tri-generation system of power, heating, and freshwater (for an industrial town) by using solar flat plate collectors, multi-stage desalination unit, and Kalina power generation cycle. *Energy Convers Manag* 2018; 165.
- [5] Mehrpooya M, Ghorbani B, Sadeghzadeh M. Hybrid solar parabolic dish power plant and high-temperature phase change material energy storage system. *Int J Energy Res* 2019; 43:5405–20.
- [6] Şenpinar A, Cebeci M. Evaluation of power output for fixed and two-axis tracking PV arrays. *Appl Energy* 2012; 92:677–85.
- [7] Koussa M, Cheknane A, Hadji S, Haddadi M, Noureddine S. Measured and modelled improvement in solar energy yield from flat plate photovoltaic systems utilizing different tracking systems and under a range of environmental conditions. *Appl Energy* 2011; 88:1756–71.
- [8] Cruz-Peragón F, Casanova-Peláez PJ, Díaz FA, López-García R, Palomar JM. An approach to evaluate the energy advantage of two axes solar tracking systems in Spain. *Appl Energy* 2011; 88:5131–42.
- [9] Al-Mohamad A. Efficiency improvements of photovoltaic panels using a Sun-tracking system. *Appl Energy* 2004; 79:345–54.
- [10] Ahmadi MH, Baghban A, Sadeghzadeh M, Zamen M, Mosavi A, Shamshirband S, et al. Evaluation of electrical efficiency of photovoltaic thermal solar collector. *Eng Appl Comput Fluid Mech* 2020; 14:545–65.
- [11] Sadeghzadeh M, Ahmadi MH, Kahani M, Sakhaeinia H, Chaji H, Chen L. Smart modeling by using artificial intelligent techniques on thermal performance of flat-plate solar collector using nanofluid. *Energy Sci Eng* 2019; 0.
- [12] Naseri A, Fazlikhani M, Sadeghzadeh M, Naeimi A, Bidi M, Tabatabaei SH. Thermodynamic and Exergy Analyses of a Novel Solar-Powered CO<sub>2</sub> Transcritical Power Cycle with Recovery of Cryogenic LNG using Stirling Engines. *Renew Energy Res Appl* 2020; 1:175–85.
- [13] Seme S, Štumberger G, Voršič J. Maximum Efficiency Trajectories of a Two-Axis Sun Tracking System Determined Considering Tracking System Consumption. *IEEE Trans Power Electron* 2011; 26:1280–90.
- [14] Kaldellis J, Zafirakis D. Experimental investigation of the optimum photovoltaic panels' tilt angle during the summer period. *Energy* 2012; 38:305–14.
- [15] Ya'acob ME, Hizam H, Khatib T, Radzi MAM. A comparative study of three types of grid connected photovoltaic systems based on actual performance. *Energy Convers Manag* 2014; 78:8–13.
- [16] Sefa İ, Demirtas M, Çolak İ. Application of one-axis sun tracking system. *Energy Convers Manag* 2009; 50:2709–18.
- [17] Mousazadeh H, Keyhani A, Javadi A, Mobli H, Abrinia K, Sharifi A. A review of principle and sun-tracking methods for maximizing solar systems output. *Renew Sustain Energy Rev* 2009; 13:1800–18.
- [18] Lee C-Y, Chou P-C, Chiang C-M, Lin C-F. Sun Tracking Systems: A Review. *Sensors (Basel)* 2009; 9:3875–90.
- [19] Kassem A, Hamad M. A microcontroller-based multi-function solar tracking system. 2011 IEEE Int. Syst. Conf., 2011, p. 13–6.
- [20] Bentaher H, Kaich H, Ayadi N, Ben Hmouda M, Maalej A, Lemmer U. A simple tracking system to monitor solar PV panels. *Energy Convers Manag* 2014; 78:872–5.

[21] Kelly NA, Gibson TL. Increasing the solar photovoltaic energy capture on sunny and cloudy days. *Sol Energy* 2011; 85:111–25.

[22] Singh GK. Solar power generation by PV (photovoltaic) technology: A review. *Energy* 2013; 53:1–13.

[23] Marefati M, Mehrpooya M, Shafii MB. Optical and thermal analysis of a parabolic trough solar collector for production of thermal energy in different climates in

Iran with comparison between the conventional nanofluids. *J Clean Prod* 2018; 175:294–313.

[24] Ibrahim HE-. A, Houssiny FF, El-Din HMZ, El-Shibini MA. Microcomputer controlled buck regulator for maximum power point tracker for DC pumping system operates from photovoltaic system. *FUZZ-IEEE'99. 1999 IEEE Int. Fuzzy Syst. Conf. Proc. (Cat. No. 99CH36315), Vol. 1, 1999, p. 406–11 Vol. 1.*

[25] Kalogirou SA. *Solar Energy Engineering: Processes and Systems.* 2009.